Picosecond spectroscopy of highly excited CdS

H. Saito* and E. O. Göbel
Max-Planck-Institut für Festkörperforschung, Heisenbergstrasse 1, 7000 Stuttgart 80, Federal Republic of Germany
(Received 17 July 1984)

Picosecond luminescence and excite-and-probe transmission as well as transient grating measurements are performed for highly excited CdS at a bath temperature of 5 K. The luminescence and the optical gain due to both the electron-hole plasma and the excitonic molecule recombination are observed. The electron-hole plasma decays very fast and disappears within 150—200 ps, whereas the excitonic molecule decays rather slowly. Both bimolecular recombination of the electrons and holes within the plasma and the diffusion of the carrier toward the low-density directions cause the decrease of the electron-hole density. In the case of a small volume of the electron-hole plasma, i.e., for rather-low-excitation levels, the transformation of the plasma into the excitonic system results in an additional shortening of the decay time of the plasma. The possibility of electron-hole liquid formation is definitely excluded.

I. INTRODUCTION

Optical properties of highly excited CdS under quasistationary conditions have been studied extensively within the last years.[1] It is well established that at a high concentration of excited electrons and holes luminescence from an electron-hole plasma (EHP) is observed. Luminescence due to excitonic molecule recombination is also observed under intermediate-excitation conditions at low temperature.[2] Picosecond spectroscopy is required to investigate the relaxation and recombination behavior of elementary excitation in direct-gap semiconductors such as CdS. Several works which have reported on picosecond spectroscopy for CdS are concerned mostly with the recombination luminescence of the EHP as well as of the excitonic molecule.[3–8] However, several problems such as the effect of transformation of the EHP to excitons and excitonic molecules (Mott transition), carrier diffusion, and possible electron-hole liquid formation on the EHP dynamics have not been considered in detail. All these processes will affect the carrier dynamics and EHP lifetime. The EHP lifetime as measured, e.g., in a time-resolved photoluminescence experiment, therefore in general is not an intrinsic property of the EHP, but instead reflects a complex average over all the processes which diminish the carrier density. It is the aim of this paper to classify the different contributions of the processes mentioned above on the EHP lifetime. This, however, can be accomplished only if different experimental techniques are applied.

We have performed time-resolved luminescence studies and two kinds of excite-and-probe studies, i.e., transmission measurements under high-intensity excitation and picosecond transient-grating measurements, to obtain further information on the dynamics of high-density electrons and holes as well as transformation of these carriers to excitons and molecules in CdS. Our results show that for high excitation ($N_{e\text{-}h} \geq 10^{18}$ cm^{-3}) the optical properties within the first 100—200 ps are governed by the EHP. The decay of the EHP is due to both carrier recombination as well as carrier diffusion and the EHP cannot be maintained for times larger than 200 ps, because it transforms into excitons and excitonic molecules. For times larger than 200 ps the optical properties are thus determined by the excitonic system. We further show that the EHP does not undergo a phase transition to an electron-hole liquid during its lifetime.

This paper will be organized as follows. In Sec. II we describe the experimental procedures for the luminescence and two kinds of excite-and-probe measurements. In Sec. III we report the results of time-resolved luminescence studies. These experiments in particular provided accurate data on the variation of the effective carrier temperature with time for different excitation conditions. Section IV deals with the results on time-resolved transmission spectroscopy under high-intensity excitation. It is well known that the optical gain spectrum of the EHP gives a direct measurement of the electron-hole pair density $N_{e\text{-}h}$. An analysis of the time-resolved optical gain spectra and the time behavior of the optical gain due to the EHP yield the time-dependent density of the electron-hole pairs in the EHP. Under intermediate-excitation conditions, optical gain due to excitonic molecule recombination and also the transformation from the EHP to excitons and excitonic molecules, are observed.

The density of the carriers inside the crystal is inhomogeneous for one-photon band-to-band excitation as employed in the present studies, i.e., the carrier density has a steep gradient normal to the excited surface because of a large absorption coefficient of about 2×10^5 cm^{-1} for the excitation laser energy. It has been shown for, e.g., GaAs, that diffusion of the carriers along the steep density gradient plays an important role in changing the spatial distribution of the carriers initially created by the photoabsorption.[9] The transient diffraction grating technique is the direct way to measure the ambipolar diffusion coefficient of free carriers. In Sec. V we report the picosecond dynamics of laser-induced transient gratings produced by direct absorption of laser pulses. The diffusion coefficient of the photogenerated carriers is obtained by measuring

the decay of the induced grating for different grating spacings.

II. EXPERIMENTAL PROCEDURES

For the measurement of spontaneous luminescence, crystals with a size of about $5\times5\times1$ mm^3 are used. By using such block crystals with large size, the luminescence is dominated by spontaneous emission, because stimulation effects can be easily suppressed.[3] These crystals have a plane perpendicular to the c axis and therefore luminescence with the polarization direction $E\perp c$ is only measured. For the excite-and-probe measurements thin platelet crystals with a thickness less than ~10 μm are used in order to minimize the background absorption (absorption without the excitation) of the probe pulses. The crystals mounted on a cold finger which was in contact with liquid He are maintained at a temperature of about 5 K.

Optical excitation was provided via one-photon band-to-band absorption of the third harmonic pulses (355 nm) of a passively mode-locked Nd—yttrium-aluminum-garnet laser (pulse width ~25 ps) for both luminescence and excite-and-probe experiments. A CS_2 optical Kerr shutter with the time resolution of ~25 ps was used in the time-resolved luminescence experiments for a picosecond light gate. The luminescence was detected using a 0.5-m grating spectrometer and an intensified photodiode linear array or a photomultiplier for spectrally resolved measurements. The time behavior of the spectrally integrated luminescence intensity was detected by using only a photomultiplier attached with an uv-cut filter. For the excite-and-probe transmission measurements the output pulses from a dye laser synchronously pumped by the third harmonic of the Nd—yttrium-aluminum-garnet laser were used as probe pulses. Coumarin 152A dissolved in p dioxane covers the wavelength range of interest between 460 and 520 nm. The dye laser was tuned by means of an interference filter and an étalon with wavelength resolution of about 0.12 nm. The excitation pulses at 355 nm were focused on the sample to a spot size of ~600 μm in diameter, whereas the probe pulses were focused to a spot size of ~200 μm, in order to monitor only the highest-excitation part of the excited area.

The time-resolved transmission spectra were obtained by measuring the transmitted probe-pulse intensity for different time delays between the excitation pulses and the probe pulses. Time evolution of the optical gain was obtained by measuring the transmitted probe-pulse intensity as a function of the time delay between the excitation and the probe pulses. The experimental configuration used in the transient-grating measurements was as follows: Two excitation pulses at 355 nm, separated by an angle of 2θ, are focused on the sample to coincide both spatially and temporally. The interference between the two pump pulses produces a modulation of the optically created carrier density to form a grating.[10] This grating decays with time due to recombination and diffusion of the carrier from the high-concentration regions to low-concentration regions. The grating decay is monitored by measuring the first-order diffracted light of a probe pulse at 532 nm (which is transparent for CdS) as a function of time delay between the excitation pulses and the probe pulses. The grating spacing is easily controlled by changing the angle 2θ between the two excitation pulses.

A single pulse was switched from the train of the mode-locked pulses by means of an electro-optic shutter for all experiments. Excitation pulses and probe pulses with almost constant amplitude are selected electronically and are used for averaging. The excitation energy of 1 μJ corresponds to a power density of ~10 MW/cm^2 throughout the present experiments.

III. LUMINESCENCE EXPERIMENTS

Figure 1 shows time-resolved luminescence spectra for band-to-band excitation with $\lambda=355$ nm. A very broad luminescence band is observed just after excitation. The broad band becomes sharper with increasing time. The spectral shape and its time evolution are in principle the same as those reported by Yoshida *et al.*[3] The spectra observed in the entire time range were ascribed to spontaneous luminescence due to the recombination of the EHP by these authors. However, the nature of the luminescence line observed in the time region later than 200 ps, where the spectra are rather sharp, is not yet clearly understood.[5] It is noticed that the position of the sharp line in the later time region coincides with the luminescence line due to excitonic molecule recombination.[2]

Figure 2 shows semilogarithmic plots of the spectrally integrated luminescence intensity versus time delay for two different excitation levels. For an excitation intensity (I_{exc}) of 0.28 μJ the luminescence intensity shows an ex-

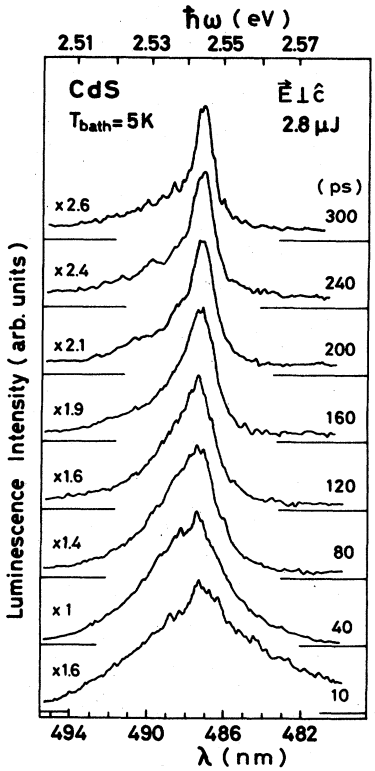

FIG. 1. Time-resolved spontaneous luminescence spectra measured at $T_{bath}=5$ K.

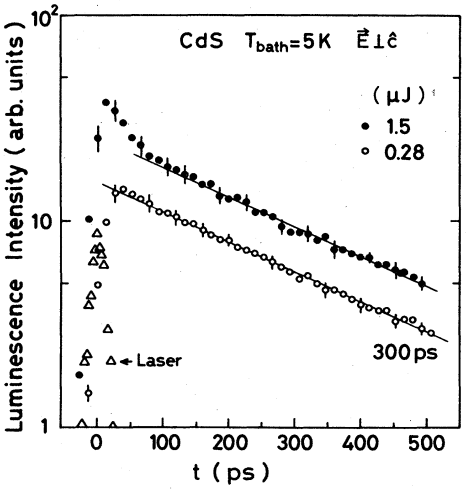

FIG. 2. Spectrally integrated spontaneous luminescence intensity as a function of delay time measured at $T_{bath}=5$ K for two excitation levels.

ponential decay with a time constant of ~ 300 ps. For $I_{exc}=1.5$ μJ a component with a fast decay begins to appear just after the excitation followed by the exponential decay with the same time constant as for $I_{exc}=0.28$ μJ. The time evolution of the luminescence intensity remains essentially the same with further increase of I_{exc} up to 8 μJ.

The fact that the luminescence decay has two components suggests that two different recombination processes contribute to the luminescence decay. The luminescence with the fast decay time disappears within about 150 ps and thereafter the luminescence with slow decay time should govern the emission spectrum. If this interpretation is applied to the luminescence spectra in Fig. 1, one can easily recognize that the luminescence with the fast decay corresponds to the broad band observed just after excitation and the luminescence with the slow decay to the sharp line in the later time regime. Therefore it is reasonable to conclude that the sharp line in the later time regime is due to the recombination of excitonic molecules because of its energetic position and linewidth, and that the broad band arises from the recombination of the EHP. The luminescence spectra in Fig. 1 can be understood as follows: The EHP created by the strong laser excitation decays rapidly and within 200 ps the EHP transforms to excitons and excitonic molecules. This interpretation is in contradiction to that proposed by Yoshida *et al.*[3–5] and will be further supported by the transmission data (Sec. IV).

For further analysis, especially of the transmission data in Sec. IV, the effective temperature (T_{eff}) of the EHP has to be known. T_{eff} can be determined from time-resolved luminescence data, because the high-energy part of the luminescence spectrum reflects T_{eff} via the respective distribution function of the electrons and the holes.[11] The effective temperatures as obtained from the high-energy part of the time-resolved luminescence spectra are shown in Fig. 3. In the early time region ($t<50$ ps) T_{eff} strongly

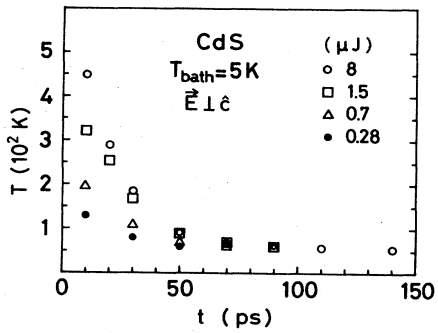

FIG. 3. Effective temperature of the EHP as a function of delay time measured at $T_{bath}=5$ K for four excitation levels.

depends on the excitation intensity. A steep decrease of T_{eff} down to 60–90 K is found within the first 50 ps, and thereafter the decrease becomes slower. It is important to note that T_{eff} does not decrease below 50 K even at 140 ps, which is still much higher than the lattice temperature. A detailed discussion of these results will be published elsewhere.

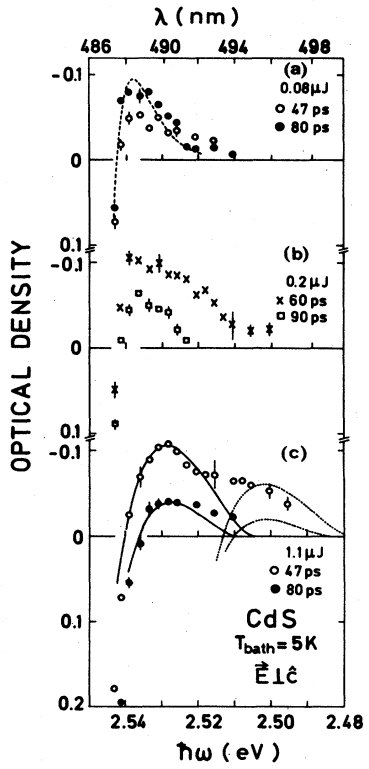

FIG. 4. Time-resolved optical density spectra measured at $T_{bath}=5$ K for three excitation levels: (a) for $I_{exc}=0.08$ μJ, (b) for $I_{exc}=0.2$ μJ, and (c) for $I_{exc}=1.1$ μJ. Negative OD value corresponds to optical gain. Solid and dotted curves in (c) are calculated gain spectra due to the EHP, and dashed curve in (a) is calculated gain spectrum due to the excitonic molecule recombination as described in the text.

IV. TRANSMISSION EXPERIMENTS

Figure 4 depicts time-resolved optical density (OD) spectra for three excitation levels. Negative OD values correspond to optical gain. For $I_{exc}=1.1$ μJ [Fig. 4(c)] the OD spectrum at 47-ps delay time has a peak at 2.528 eV accompanied by a shoulder at 2.52—2.49 eV. The peak value of the gain coefficient is about 5600 cm^{-1}, if we assume a depth of the excited volume to be 0.5 μm. This point will be discussed further in Sec. V. The OD value itself decreases with increasing time (80 ps). The crossover position from absorption to gain is situated at 2.540—2.536 eV and shifts to lower energies with time. For $I_{exc}=0.2$ and 0.08 μJ [Figs. 4(b) and 4(a)], the peak position is situated at about 2.536 eV. The crossover position of 2.541—2.542 eV is slightly higher than for $I_{exc}=1.1$ μJ. It should be noted that the crossover position is identical and remains almost unchanged with time in contrast to $I_{exc}=1.1$ μJ. For $I_{exc}=0.2$ μJ the spectral width of the OD curve decreases rapidly with time and amounts to 20 meV at 90 ps. Instead, the spectral width is narrow (20 meV) for $I_{exc}=0.08$ μJ in the entire time regime.

Further information on the dynamical behavior of the various processes contributing to the OD spectrum can be gained by observing the time dependence of the OD at fixed energies as shown in Figs. 5—7. The spectral position of $\hbar\omega=2.531$ eV (Fig. 5) is close to the peak of the gain spectrum for $I_{exc}=1.1$ μJ shown in Fig. 4(c). The optical gain observed at the instant of the excitation increases for $I_{exc}=1.1$ μJ within the first 40 ps and then decays with the decay constant of about 60 ps, if an exponential decay is assumed (solid circles). The OD value at the peak (about -0.14) corresponds to a gain coefficient of 6400 cm^{-1}, using again a depth of the excited volume of 0.5 μm. For $I_{exc}=0.2$ μJ (open circles) and 0.08 μJ (triangles) shown in Fig. 5, absorption takes place just after the excitation (not shown in Fig. 5). This absorption changes to gain at 30—40 ps. The decay constant of the gain for $I_{exc}=0.08$ μJ is about 110 ps.

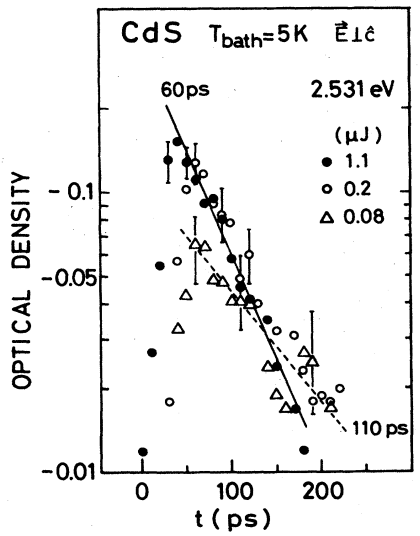

FIG. 5. Optical gain at $\hbar\omega=2.531$ eV as a function of delay time between the excitation pulse at $\lambda=355$ nm and the probe pulse at $\lambda=489.7$ nm (2.531 eV) for three excitation levels. Solid line indicates the decay time of 60 ps and dashed line of 110 ps.

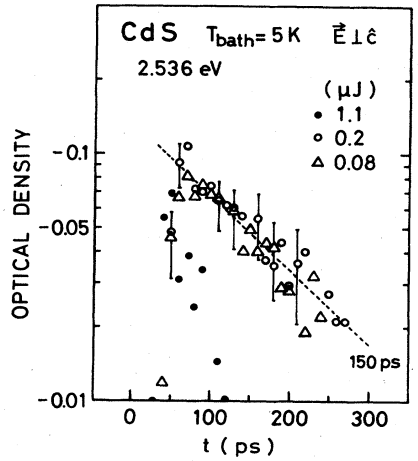

FIG. 6. Optical gain at $\hbar\omega=2.536$ eV as a function of delay time between the excitation pulse at $\lambda=355$ nm and the probe pulse at $\lambda=488.7$ nm (2.536 eV) for three excitation levels. Solid line indicates the decay time of 150 ps.

The time variation of the transmission signal at the position of $\hbar\omega=2.536$ eV, which is near the peak of the gain spectra for $I_{exc}=0.2$ and 0.08 μJ, is depicted in Fig. 6. Absorption observed just after the excitation also changes to gain at about 40 ps. The gain decays with a decay constant of about 150 ps for both $I_{exc}=0.2$ and 0.08 μJ and extends for longer times than for $I_{exc}=1.1$ μJ, where optical gain is observed only at a very early stage.

Figure 7 finally depicts the time variation of the OD for $\hbar\omega=2.539$ eV. A linear plot of the OD values is chosen in this case (opposite to Figs. 5 and 6) because the position of $\hbar\omega=2.539$ eV is close to the zero crossover of the spectra. Absorption observed just after the excitation

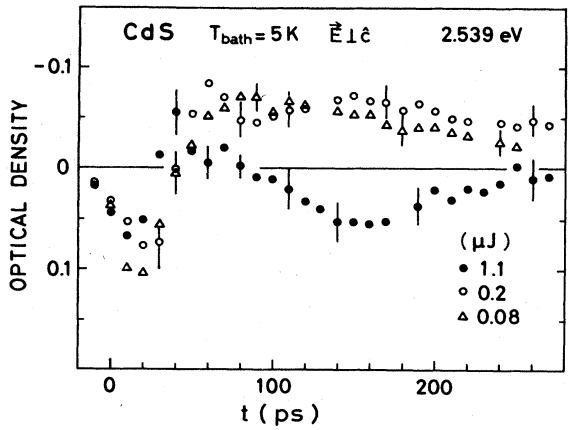

FIG. 7. Optical density at $\hbar\omega=2.539$ eV as a function of delay time between the excitation pulse at $\lambda=355$ nm and the probe pulse at $\lambda=488.1$ nm (2.539 eV) for three excitation levels. Negative OD values again correspond to optical gain.

again changes to gain at 30—40 ps for all excitation intensities. The optical gain decays smoothly with a time constant of about 180 ps for $I_{exc}=0.08$ μJ. For $I_{exc}=1.1$ μJ, however, the gain decreases rapidly and changes to absorption at about 80 ps. This behavior corresponds to the shift of the crossover position to the low-energy side as observed for $I_{exc}=1.1$ μJ in Fig. 4(c). In the time region which is later than 150 ps the absorption tends to decrease again. The time behavior for $I_{exc}=0.2$ μJ is considered to be the superposition of the low- and high-excitation results, that is, the time behavior until $\sim$100 ps roughly corresponds to that of $I_{exc}=1.1$ μJ and after $\sim$100 ps it is very similar to that for $I_{exc}=0.08$ μJ.

Summarizing the results of Figs. 4—7, the low-energy broad band peaked at $\hbar\omega=2.528$ eV observed for high excitation decays rapidly and disappears within 200 ps. The crossover position, simultaneously, shifts to the low-energy side with time. The high-energy band peaked at about $\hbar\omega=2.536$ eV, which is observed for low excitation, on the other hand, decays rather slowly and the crossover position does not shift with time. This difference in time behavior between the two gain bands implies that each gain band originates from different recombination processes. The temporal behavior of the gain for the intermediate excitation ($I_{exc}=0.2$ μJ) in the early stage reflects the superposition of the two gain processes. The low-energy broad band disappears within $\sim$100 ps, and thereafter only the high-energy band is observed.

The recombination process both due to the EHP and the excitonic molecule should contribute to optical gain. However, it is difficult to distinguish between these two processes under a quasistationary condition, because their spectral position almost coincides. The two processes, however, can be distinguished by their different time behavior[12] as shown before. The optical gain observed for $I_{exc}=0.08$ μJ is therefore attributed to excitonic molecule recombination. We further conclude that the broad gain band with the faster decay time observed for $I_{exc}=1.1$ μJ is due to the recombination of the EHP. The high peak gain value of 5600—6400 cm^{-1} is also consistent with this interpretation.

We now will discuss the results for $I_{exc}=1.1$ μJ in more detail. As shown in the data of Fig. 3, T_{eff} for $I_{exc}=1.1$ μJ is about 250—300 K at 10-ps delay time and decreases to about 80 K at 50 ps. This decrease in T_{eff} results in a high-energy shift of the chemical potential of the EHP if $N_{e\text{-}h}$ remains constant. Experimental results in Fig. 4(c), on the contrary, show a low-energy shift of the crossover position, which corresponds to the chemical potential of the EHP.[13] This fact definitely rules out the possibility of electron-hole liquid formation even after 50 ps, where T_{eff} is around the critical temperature for liquid formation of 65 K.[14] We instead show that $N_{e\text{-}h}$ decreases continuously because of the recombination and the diffusion of the carrier (see also Sec. V).

$N_{e\text{-}h}$ is obtained by analyzing the gain spectra in Fig. 4(c). Calculations are performed with the simplified assumption that the $\vec{k}$ selection rule for the recombination of electrons and holes in the EHP can be neglected.[15] The effective temperatures at 47 and 80 ps used for the calculation were 80 and 65 K, respectively, as given in Fig. 3. The results of this simplified calculation are shown by solid curves in Fig. 4(c). $N_{e\text{-}h}$ used for the calculation is 2.8×10^{18} cm^{-3} for the spectrum at 47 ps. It is obvious that the low-energy part of the spectrum cannot be fitted. The low-energy part, however, can be attributed to a coupled plasmon-phonon sideband of the main EHP emission as pointed out previously.[16,17] For $N_{e\text{-}h}=2.8\times10^{18}$ cm^{-3} the energy of the lower branch of the plasmon-phonon mode amounts to 27 meV. We thus have plotted a replica of the main EHP band shifted by 27 meV by the dotted curve. The intensity of the dotted curve has been chosen to fit the experimental data, when superimposed to the main EHP band. Good agreement between the experimental points at 47 ps and the calculated gain curve is obtained with this procedure. The high-energy part of the OD spectrum at 80 ps can be fitted with $N_{e\text{-}h}=1.9\times10^{18}$ cm^{-3}, but again the spectrum is much broader than expected without taking into account a plasmon-phonon replica. We therefore conclude that the rather broad gain spectrum at 47 and 80 ps can be attributed to the occurrence of a plasmon—LO-phonon coupled mode sideband of the main EHP recombination band.

The recombination of the electron and the hole in the EHP represents a bimolecular recombination process. The recombination rate is thus given by $R_{rec}=\beta(N_{e\text{-}h})^2$, where β is the bimolecular recombination coefficient. Using $N_{e\text{-}h}$ at 47 and 80 ps, we can estimate β to be $5\text{—}7\times10^{-9}$ cm^2/s.

An accurate energy diagram is necessary for further discussion. Several calculated results have been published so far,[14,18] but unfortunately none of them is in accordance with the present experimental results. For instance, according to the result by Rösler and Zimmermann,[14] the EHP with $T_{eff}=80$ K and the chemical potential at $\hbar\omega=2.540$ eV, which is the experimental result at 47 ps, should have a density of more than 10^{19} cm^{-3}. This density is drastically higher than the value of 2.8×10^{18} cm^{-3}, estimated from our data. We therefore restrict outselves to a qualitative discussion based on the energy diagram as given in Fig. 8.

The calculation of the energy diagram of the EHP as shown in Fig. 8 was performed in a simple manner in which the interaction between the carriers and LO phonons is ignored. Therefore the ground-state energy (E_0) is given simply by the sum of the kinetic energy of the electron and the hole, exchange energy between them, and correlation energy.[19] The kinetic and the exchange energies as a function of r_s defined via $N_{e\text{-}h}=3/(4\pi r_s^3 a_{ex}^3)$ (a_{ex} is the exciton Bohr radius) are calculated in the standard manner with the parameters given below. The correlation energy is obtained from the results of Vashishta *et al.*,[20] where the correlation energy has been calculated self-consistently for a mass ratio $m_{dh}/m_e=6$ and for r_s between 0.2 and 2; m_e is the electron mass and m_{dh} is the density-of-state mass of $m_{h\parallel}$ and $m_{h\perp}$, where $m_{h\parallel}$ and $m_{h\perp}$ are the hole mass parallel and perpendicular to the c axis of CdS, respectively. The masses used for the calculation are band effective masses which were evaluated from effective polaron masses by Beni and Rice,[18] and are as follows: $m_e=0.185m_0$, $m_{h\parallel}=4.38m_0$, and $m_{h\perp}=0.555m_0$, and therefore $m_{dh}=1.105m_0$ and the ratio

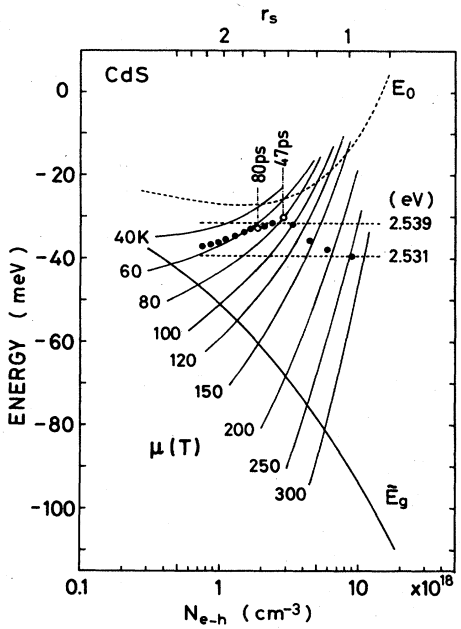

FIG. 8. Calculated chemical potential of the EHP (μ) for several temperatures and renormalized band gap ($\tilde{E}_g$) as a function of $N_{e\text{-}h}$. Open circles indicate the observed chemical potential at 47 and 80 ps. The solid circles indicate the calculated position of the chemical potential at different times as described in the text. From the right-hand to the left-hand side of the figure the calculated points (solid circles) correspond to 10, 20, 30, 40, 60, 70, 90, 100, 120, 140, 160, 180, and 200 ps. Dashed lines are the energy positions for the observed OD at $\hbar\omega=2.531$ and 2.539 eV.

$m_{dh}/m_e=0.597$. With use of these masses and a static dielectric constant of 8.58, a_{ex} is calculated to be 3.03 nm. $N_{e\text{-}h}$ corresponding to $r_s=2$ and 0.2 amount to 1.07×10^{18} cm^{-3} and 1.07×10^{21} cm^{-3}, respectively. The correlation energies for $r_s>2$ were estimated by extrapolating the values for $r_s<2$ using the approximation that the correlation energy can be expressed by a quadratic function of $1/r_s$. The validity of the calculated energy diagram for $r_s>2$ is therefore questionable, but as will be shown later most of the experimental values for the densities fall within the region of $r_s<2$. The renormalized band gap ($\tilde{E}_g$) and the chemical potential (μ) at given $N_{e\text{-}h}$ and T_{eff} then are easily calculated on the basis of the results for the ground-state energy.

The energy diagram should satisfy the following condition to be consistent with our experimental results: The chemical potential for $N_{e\text{-}h}=2.8\times10^{18}$ cm^{-3} and $T_{eff}=80$ K should be at $\hbar\omega=2.540$ eV and for $N_{e\text{-}h}=1.7\text{–}2\times10^{18}$ cm^{-3} and $T_{eff}=65$ K at $\hbar\omega=2.536$ eV. It is found that this condition is satisfied if the calculated energy diagram is shifted rigidly towards the low-energy direction by an amount of 6 meV.[21] The corresponding results for the ground-state energy E_0, the band gap $\tilde{E}_g$, and the chemical potential $\mu(T)$ are depicted in Fig. 8 together with the experimental data. The open circles represent the experimental data for $I_{exc}=1.1$ μJ at delay times of 47 and 80 ps. The position of the chemical potential μ now can be calculated at any delay time with the known value for the bimolecular recombination coefficient ($\beta\simeq6\times10^{-9}$ cm^3/s) and the experimental results for T_{eff} versus time. The calculated values for μ are also depicted in Fig. 8 by solid circles for time delay between 10 and 200 ps. The high-energy shift of the chemical potential within the first 50 ps is caused by both the decrease of T_{eff} and of $N_{e\text{-}h}$ with time. The position of the chemical potential in turn moves to the low-energy direction in the time range later than 50 ps nearly along the curve for the chemical potential with $T_{eff}=60$ K, because T_{eff} is almost constant in this time region (cf. Fig. 3).

The time behavior of the OD at $\hbar\omega=2.531$ eV corresponding to Fig. 5 and $\hbar\omega=2.539$ eV corresponding to Fig. 7 can also be explained on the basis of Fig. 8. The respective energies are shown in Fig. 8 by the dashed lines. When the observed energy is situated below or above the chemical potential in Fig. 8, optical gain or absorption should be observed, respectively. Thus gain should be observed for $\hbar\omega=2.539$ eV in the time regime of 40—60 ps and absorption should take place within the first 40 ps and after 60 ps. This exactly explains the time behavior of the OD for $I_{ex}=1.1$ μJ shown in Fig. 7. On the other hand, for $\hbar\omega=2.531$ eV (Fig. 5), gain should be observed within the entire time range up to 200 ps. The fast cooling of the EHP in the early stage is responsible for the rise of the gain value, whereas the decrease of the gain values after 50 ps is due to the decrease of $N_{e\text{-}h}$.

Summarizing the results for $I_{exc}=1.1$ μJ, the OD spectra and the time behavior of the OD are well explained by the recombination of the electron and the hole in the EHP. The formation of electron-hole liquid does not take place and the EHP created under this excitation intensity decays with a bimolecular recombination rate of $5\text{–}7\times10^{-9}$ cm^2/s, and disappears within 200 ps.

Next we will discuss the results observed for $I_{exc}=0.08$ μJ. The observed gain for this excitation intensity is ascribed to excitonic molecule recombination. If we assume that the excitonic molecule and the free exciton are at the same temperature (T), their distributions can be described by Boltzmann statistics. The optical gain spectrum $G(\hbar\omega)$ associated with the recombination of the excitonic molecule is obtained by a simple calculation in which the $\vec{k}$ dependence of the matrix element is neglected and is given by

$$G(\hbar\omega)\propto T^{-3/2}(E_m-\hbar\omega)^{1/2}\left[\left[\frac{1}{2}\right]^{3/2}\left[\frac{N_m}{N_{ex}}\right]e^{-(E_m-\hbar\omega)/k_BT}-e^{-2(E_m-\hbar\omega)/k_BT}\right], \quad (1)$$

where N_m and N_{ex} are the density of the excitonic molecules and the excitons, respectively. $E_m=E_{ex}-E_m^b$, where E_{ex} is the energy of the free exciton and E_m^b is the binding energy of the excitonic molecule. One easily finds that the crossover position from absorption to gain, which is given by solving $G(\hbar\omega)=0$ except for the case of

$\hbar\omega = E_m$, is a function of the ratio N_m/N_{ex} and T. The experimental result in Fig. 4(a) gives the crossover at $\hbar\omega = 2.5424$ eV. If we use $E_m = 2.5473$ eV,[22] resulting in $E_m - \hbar\omega = 4.9$ meV, and $T = 60$ K, Eq. (1) yields the ratio N_m/N_{ex} to be about 1.1. The calculated gain spectrum due to exciton molecule recombination is also depicted in Fig. 4(a) by the dashed curve, where the only fitting parameter is the absolute OD value. Good agreement is found, giving a confirmation of the present interpretation.

One also finds from Eq. (1) that the crossover shifts to the high-energy side with decreasing T and with the increasing ratio N_m/N_{ex}. The spectral width is very sensitive to T but not to the changes of the ratio N_m/N_{ex}. The width becomes narrower with decreasing T. The observed slight decrease of the half-width of the OD curves for 80 ps compared to 40 ps in Fig. 4(a) thus indicates that the excitonic temperature T still decreases somewhat within this time regime. The shift of the crossover position can be discussed on the basis of data shown in Fig. 7 (triangles). The change of adsorption into gain at about 40 ps after excitation can be attributed to a shift of the crossover position to higher energies which can be caused by both the decrease of temperature and an increase of N_m/N_{ex} due to the finite exciton molecule formation time. For $t > 80$ ps, N_m/N_{ex} is determined by T only and the decrease of the gain values can be attributed to a decrease of the molecule (and exciton) density. According to Eq. (1) the decay of the gain, furthermore, should be faster at the low-energy side compared to the high-energy side because of the decrease of T. This is also observed experimentally as shown in Figs. 5 and 6, where for $I_{exc} = 0.08$ μJ the decay constant for $\hbar\omega = 2.531$ eV is about 110 ps (Fig. 5) and increases to about 150 ps for $\hbar\omega = 2.536$ eV.

Under resonant excitation of the excitonic molecule, in which almost no excitons are excited directly, the excitonic molecule luminescence shows an extremely short lifetime of about 20 ps.[7] In the present case, however, the exciton and the excitonic molecule are created via low-density carriers excited by band-to-band absorption. Because of the extremely short lifetime of the excitonic molecule, N_m is determined by the longer exciton lifetime and molecule formation time, resulting in a slower decay of N_m. This causes the slow decay of the luminescence as well as the optical gain due to the excitonic molecule recombination.

Based on the discussion made for high- and low-excitation cases, we will consider the case of $I_{exc} = 0.2$ μJ. The gain spectrum at 60 ps in Fig. 4(b) for this excitation intensity is the superposition of the gain due to the EHP in the low-energy part and the gain due to the excitonic molecule in the high-energy part. The crossover position in this case is determined by that of the excitonic molecule. After disappearance of the EHP, the gain spectrum coincides with that due to the excitonic molecule recombination as seen in the spectrum at 90 ps. A similar discussion can be made for the time behavior of the gain, i.e., at a position where the gain due to the EHP is strong the time behavior in the early stage is governed by that of the EHP, and after disappearance of the EHP the decay of the gain coincides with decay of the excitonic molecule as seen in Figs. 5 and 7. On the other hand, the time behavior at $\hbar\omega = 2.536$ eV (Fig. 6), where almost no gain due to the EHP is present, is governed by that of the excitonic molecule, and therefore the gain shows a slower decay time in the entire time regime.

The fact, that the gain due to both the EHP and the excitonic molecule is observed at the same time, indicates that the probe beam covers the region occupied by the EHP as well as by excitons and excitonic molecules. This means that probably only the central part of the excitation beam and the part very close to the surface is occupied by the EHP, and most part of the excited region is occupied by the excitons and the excitonic molecules. It seems very likely that for this case transformation from the EHP to the exciton and the excitonic molecule at their interface plays an important role in decreasing the volume occupied by the EHP, resulting in a further shortening of the lifetime of the EHP. This causes the EHP to disappear faster than for $I_{exc} = 1.1$ μJ.

Summarizing, the transmission experiments can be well explained by taking into account the interplay between the EHP and the excitonic system. At the highest-excitation intensities the time behavior of the OD initially is dominated by the EHP, whereas for $I_{exc} = 0.08$ μJ only the excitonic molecule contributes to gain and absorption. For intermediate densities the initially created EHP rapidly transforms into excitons and excitonic molecules, resulting in a further shortening of the EHP lifetime.

V. TRANSIENT-GRATING EXPERIMENTS

As already shown in the preceding sections, the optical gain due to the EHP recombination is observed in the transmission studies for $I_{exc} = 0.2$ μJ, while in the luminescence studies no fast decay is observed even for $I_{exc} = 0.28$ μJ, indicating that no EHP is excited. This discrepancy may suggest that fast diffusion of the excited carriers into the bulk crystal causes a lowering of the effective carrier density. For the 1-mm-thick sample as used for the luminescence study, the lowering of the density due to carrier diffusion thus could be so fast that no EHP could be created. On the other hand, for the thinner sample of ~ 10 μm, which was used for the transmission study, the diffusion may be limited by the back surface and the effective density may be still sufficiently high to form the EHP. The importance of carrier diffusion under the present experimental conditions therefore must be known quantitatively in order to explain the data.

In this section results on the carrier diffusion experiments measured by means of an excite-and-probe transient-grating method will be shown. The diffraction of the probe beam is due to a free-carrier-induced index modulation of the sample. The excitation pattern at the crystal surface is given by

$$I(x) = I_0[1 + \cos(2\pi x/\Lambda)] ,$$

where Λ is the grating spacing which is given by $\Lambda = \lambda_p/2\sin\theta$ (λ_p is the wavelength of the pump laser) and I_0 is the mean excitation intensity. The excited carrier density at the peak of the grating becomes twice that in the transmission (luminescence) experiments if the

same I_0 is used for both experiments. The excitation intensity used here, therefore, was about one-half of that for $I_{exc}=1.1$ μJ in the transmission study to get the same peak carrier density in both experiments.

Figure 9 depicts semilogarithmic plots of the diffraction intensity against time measured at $T_{bath}=5$ K for three grating spacings. The decay of the diffraction intensity in Fig. 9 is nonexponential and furthermore becomes faster with decreasing grating spacing. The fact that the decay is nonexponential can be attributed to the bimolecular recombination of the EHP. The fact that the decay of the grating depends on the grating spacing Λ clearly reveals that diffusion of the carriers contributes to the decay of the grating and hence to the decrease of the EHP density. Therefore the kinetics of the plasma grating is given by

$$\frac{\partial N(x,z,t)}{\partial t}=G(x,z,t)+\vec{\nabla}[D\vec{\nabla}N(x,z,t)]-\beta N^2(x,z,t)\ , \tag{2}$$

where D is the ambipolar diffusion coefficient, β is the bimolecular recombination rate, $N(x,z,t)$ is the electron-hole pair density, and z the direction normal to the surface. The spatially modulated generation rate is given by

$$G(x,z,t)=G_0(t)[1+\cos(2\pi x/\Lambda)]\exp(-\alpha z)\ ,$$

where $G_0(t)$ is the time-dependent generation rate and is given by

$$G_0(t)=G_0/\cosh(2.634t/\tau_p)\ \ (\tau_p=25\text{ ps})\ .$$

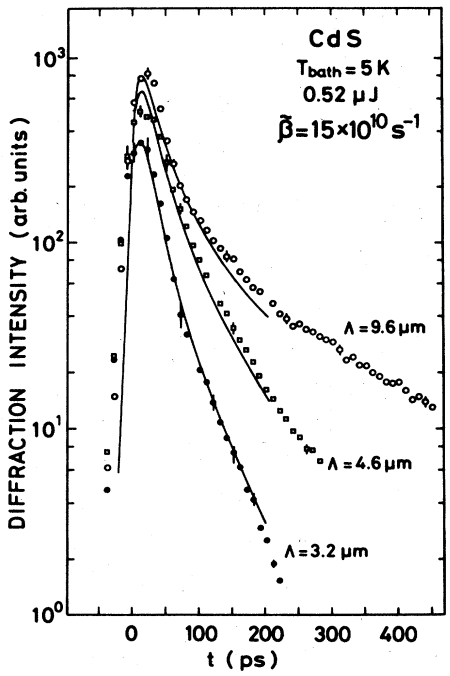

FIG. 9. Diffraction intensity as a function of delay time between the excitation pulse at $\lambda=355$ nm and the probe pulse at $\lambda=532$ nm for three grating spacings measured at $T_{bath}=5$ K. Solid curves are the calculated diffraction intensities as described in the text.

Surface recombination is not explicitly taken into account which, however, does not affect the conclusions drawn for the diffusion of the EHP. Instantaneous diffraction efficiency is proportional to the square of the first-order Bessel function $J_1^2[\phi(t)]$. $\phi(t)$ is given by [10]

$$\phi(t)=-\frac{e^2\lambda}{8\pi c^2 n m^* \epsilon_0}\int_0^\infty dz\left[N(0,z,t)-N\left[\frac{\Lambda}{2},z,t\right]\right]\ , \tag{3}$$

where λ is the wavelength of the probe pulse, n is the index of refraction, c is the velocity of light in vacuum, e is the charge of the electron, m^* is the reduced effective mass, and ϵ_0 is the permittivity constant. In the present case, because $\phi(t)\ll 1$, $J_1^2[\phi(t)]$ is approximated by $[\phi(t)/2]^2$, and therefore the instantaneous diffraction efficiency is given by $\phi^2(t)$.

In solving Eq. (2) we assumed that D is density (and therefore position) independent. We define dimensionless electron-hole density, $n(x,z,t)$ by $n(x,z,t)=N(x,z,t)/N_0$, where N_0 corresponds to the electron-hole density at $x=0$ and $z=0$ if the excitation is given by the δ function at $t=0$. Equation (2) then can be rewritten using $n(x,z,t)$, in which the bimolecular recombination rate is reduced to $\tilde{\beta}=\beta N_0$, and $G_0(t)$ to $N_0G_0(t)/\int_{-\infty}^{\infty}G_0(t)dt$.

The initial distribution of the excited carrier into the z direction, which is determined by the absorption coefficient α, is the same for the transient-grating measurement and the transmission measurement, because the excitation was provided by the same laser wavelength ($\lambda=355$ nm) for both cases. It should be noticed that the carrier diffusion normal to the excited surface takes place also in the case of the transmission measurement. This means that the value for β as obtained from the transmission experiments [$\beta=(5-7)\times10^{-9}$ cm^3/s] accounts for the lowering of the electron-hole density due to the recombination, but also due to the carrier diffusion, which is inevitably included. Therefore it makes no sense to use the real absorption coefficient at the excitation laser energy, $\alpha=2\times10^5$ cm^{-1}, together with the value of β as obtained from the transmission data.

We instead have to calculate the decay of the grating, using an appropriate absorption coefficient which should be smaller than the real value. The diffusion-recombination equation for n is then solved numerically using D and $\tilde{\beta}$ as parameters. The solid curves in Fig. 9 depict the result for $\alpha=5\times10^4$ cm^{-1}, $\tilde{\beta}=15\times10^{10}$ s^{-1}, and $D=10$ cm^2/s. This $\tilde{\beta}$ value gives $N_0=2.5\times10^{19}$ cm^{-3}, using $\beta=6\times10^{-9}$ cm^3/s. We found that the peak value for n is of about 0.31 at $x=0$, $z=0$, and $t=8$ ps, which results in the peak electron-hole density at 8 ps being $N(0,0,8)=7.7\times10^{18}$ cm^{-3}. We also found that the electron-hole density at 47 ps is $N(0,0,47)=3.2\times10^{18}$ cm^{-3}, which is nearly the same as that obtained from the transmission measurement (2.8×10^{18} cm^{-3} at 47 ps). Good agreement is found between the calculated and observed results for $t<200$ ps. The deviation for $\Lambda=9.8$ μm and $t\geq200$ ps seems to be due to the fact that the EHP disappears and transforms to excitonic system in this time regime, resulting in a possible change of D.

It should be noted that according to Eq. (3) the diffrac-

tion of the probe beam is dominated by the carrier distribution close to the surface, where the density is highest. The actual value for α therefore does not enter critically into the calculations. On the other hand, the value for D can be obtained quite accurately, because diffusion is particularly important at the sample surface where the concentration gradients are highest.

The diffusion coefficient can be also estimated from the observed Hall mobility of electrons in CdS with use of the Einstein relation. The diffusion coefficient for the electron (D_e) calculated with a Hall mobility of 10^4 cm^2/V s at 40 K (Ref. 23) is 34.5 cm^2/s. The mobility of the electron (μ_e) is given by the equation $\mu_e = e\tau_c/m_e^*$, where τ_c is collision time. By assuming the same collision time for holes, the relation $\mu_h = (m_e^*/m_h^*)\mu_e$ is obtained. Using the density-of-state mass for the hole as mentioned above, we find the Hall mobility for the holes to be $\sim 1.7\times 10^3$ cm^2/V s and a diffusion coefficient for the holes (D_h) of about 5.7 cm^2/s. The ambipolar diffusion coefficient (D) is given by $1/D = (1/D_e + 1/D_h)/2$ and thus amounts to 9.8 cm^2/s, which is very close to the value obtained from the grating experiments.

The present calculation also shows that the electron-hole density at 2 μm depth and at 150—200 ps is below 10^{16} cm^{-3}, i.e., about 2 orders of magnitude smaller than the density at the surface and already well below the Mott density. An EHP thus cannot be generated for more than 2-μm depth under the present experimental conditions. The experimentally determined value for the ambipolar diffusion coefficient $D \sim 10$ cm^2/s results in a maximum carrier velocity of 1.2×10^5 cm/s.[24,25] As shown by Forchel *et al.*,[9] the width, i.e., the position of the chemical potential, as well as the absolute values of the gain spectra can be significantly influenced by fast diffusion of the carriers. The maximum gain values and the spectral width strongly decrease for velocities above 10^6 cm/s. For the estimated velocities of about 10^5 cm/s, however, the gain spectra are almost unaffected. The rather low velocities of the carriers in CdS, on the other hand, results in a relative small EHP volume. The mean penetration depth amounts to 0.2 μm for an EHP lifetime of 200 ps. The maximum gain values given in Sec. IV therefore represent a lower limit, because they have been obtained for an effective EHP depth of 0.5 μm, and indeed maximum gain values of the order of 10^4 cm^{-1} are expected on the basis of corresponding absorption data without carrier diffusion.

Fast diffusion of carriers thus cannot explain the observed discrepancy in the excitation intensity between the transmission and the luminescence experiments. The difference, however, can be attributed to the different experimental conditions in the transmission and the luminescence experiments. The diameter of the probe beam used in the transmission study was about one-third of that of the excitation beam spot size. The transmitted beam thus essentially probes the high-density part within one-third of the excitation diameter. On the other hand, luminescence arises from the whole excited area. i.e., an appreciable contribution from the peripheral part of the excited area, where the excitation intensity is weak, is inevitably included in luminescence. In order to express this argument more quantitatively, we discuss a numerical example. We have shown in Sec. IV that for $I_{\rm exc} = 0.2$ μJ the transmission data just reveal the existence of the EHP. We therefore considered that only the central part of the excitation beam area and therefore a part very close to the excited surface is occupied with the plasma for this excitation intensity. For instance, we assume that the plasma is created within the region of $r_0/4$, where the intensity decreases to $0.9I_0$ (r_0 equals width of the Gaussian beam, I_0 equals intensity at the center). An increase of the excitation intensity by a factor of, e.g., 1.4, corresponding to $I_{\rm exc} = 0.28$ μJ, will result in increase of the radius where the EHP exists to about $0.45r_0$. The area within $0.45r_0$, however, corresponds only to 20% of the whole excited area, and about 30% of the number of excited carriers. This fact in turn means that luminescence due to the plasma recombination takes part in a minor portion of the entire excited area. The luminescence of the EHP therefore still will be masked by the strong luminescence due to the excitonic molecule recombination, and the fast decay component cannot be observed in the decay of the spectrally integrated luminescence intensity consistent with the data shown in Fig. 2.

VI. SUMMARY

The time behavior of highly excited CdS is studied with picosecond time resolution by luminescence, transmission, and transient-grating experiments. Luminescence and optical gain due to both recombination of the electron-hole plasma and exciton molecules is definitely identified. In contrast to quasistationary experiments these two recombination processes can be clearly distinguished by their different time behavior.

The EHP is created only at the highest-excitation levels and decays very fast within 100—200 ps by recombination, diffusion, and formation of excitons and exciton molecules. The time dependence of the spectral shape of the induced transmission (gain) is well explained on the basis of the energy diagram of the EHP taking into account plasmon-phonon sideband emission. The density of the EHP decreases continuously with time and the formation of an electron-hole liquid is definitely excluded. The bimolecular recombination rate for electron-hole recombination within the EHP is determined to $\beta \simeq (5-7)\times 10^{-9}$ cm^3/s. The effective temperature of the EHP increases with excitation intensity in the early time regime ($t < 50$ ps), and is almost independent on excitation intensity afterwards due to the efficient cooling by the LO phonons.

Transient-grating measurements point out that diffusion of the optically excited carriers into the low-density regimes also contributes to the decrease of the EHP density. An ambipolar diffusion coefficient of $D \simeq 8-10$ cm^2/s is obtained from a fit of the numerical solution of the continuity equation to the experimental data. The diffusion coefficient results in maximum velocities of the carriers of $\sim 10^5$ cm/s. No appreciable modification of the gain spectra due to fast carrier motion therefore is expected, contrary to the findings for, e.g., GaAs.

The time variation of the optical properties is deter-

mined by the exciton and exciton molecule at the lower-excitation level. The position and spectral shape of the optical gain observed at these excitation levels can be well explained by exciton molecule recombination.

For intermediate-excitation intensities only a small portion of the entire excited area is occupied by an EHP. The lifetime of the EHP under these conditions is further reduced due to the formation of excitons and exciton molecules at the interface.

In conclusion, our picosecond experiments have shown that the exciton system is quite stable in CdS at low temperatures. An electron-hole plasma can be created by picosecond pulses only at very high peak intensities. The lifetime of the EHP even then is very short because it rapidly transforms into the exciton system. Electron-hole liquid formation therefore cannot be expected for CdS and indeed can be excluded definitely on the base of the present results.

ACKNOWLEDGMENTS

The authors gratefully acknowledge Professor H. J. Queisser, Professor S. Shionoya, and Dr. S. Tanaka for helpful discussions. We are also indepted to Mr. H. Klann and K. Rother for their expert technical support and to Mr. H. Sawami for the numerical calculation of the nonlinear recombination-diffusion equation.

---

*Present address: Department of Applied Physics, Okayama University of Science, Ridaicho, Okayama 700, Japan.

[1]C. Klingshirn and H. Haug, Phys. Rep. **70**, 315 (1981).

[2]S. Shionoya, H. Saito, E. Hanamura, and O. Akimoto, Solid State Commun. **12**, 223 (1973).

[3]H. Yoshida, H. Saito, S. Shionoya, and V. B. Timofeev, Solid State Commun. **33**, 161 (1980).

[4]H. Yoshida, H. Saito, and S. Shionoya, J. Phys. Soc. Jpn. **50**, 881 (1981).

[5]H. Yoshida and S. Shionoya, Phys. Status Solidi B **115**, 203 (1983).

[6]A. Cornet, J. Collet, T. Amand, M. Pugnet, B. S. Razbirin, and G. Michailov, J. Phys. Chem. Solids **44**, 53 (1983).

[7]R. Baumert, Phys. Rev. B (to be published).

[8]C. V. Shank, D. H. Auston, E. P. Ippen, and O. Teschke, Solid State Commun. **26**, 567 (1978).

[9]A. Forchel, H. Schweizer, and G. Mahler, Phys. Rev. Lett. **51**, 501 (1983).

[10]A. L. Smirl, S. C. Moss, and J. R. Lindle, Phys. Rev. B **25**, 2645 (1982).

[11]W. Graudszus and E. O. Göbel, in *Proceedings of the 16th International Conference on the Physics of Semiconductors* [Physica (Utrecht)**117& 118B**, 555 (1983)].

[12]For resonant excitation of the excitonic molecule, the lifetime of the excitonic molecule is very fast, ~20 ps (Ref. 7).

[13]If the diffusion of the carrier in the EHP is important, the shift of the chemical potential is also related to the velocity of the carriers, see Ref. 9. As will be shown in Sec. V, diffusion of the carrier, though certainly present, will not influence the spectra appreciably.

[14]M. Rösler and R. Zimmermann, Phys. Status Solidi B **83**, 85 (1977).

[15]The density and temperature data obtained from a "no $\vec{k}$ selection-rule fit " are in good agreement with the data obtained by the exact calculations. H. Haug and D. B. Tran Thoai, Phys. Status Solidi B **98**, 581 (1980).

[16]E. O. Göbel, P. H. Liang, and D. v. d. Linde, Solid State Commun. **37**, 609 (1981).

[17]H. Saito, Solid State Commun. **39**, 71 (1981).

[18]G. Beni and T. M. Rice, Phys. Rev. Lett. **37**, 874 (9176); Phys. Rev. B **18**, 768 (1978).

[19]T. M. Rice, in *Solid State Physics,* edited by H. Ehrenreich, F. Seitz, and D. Turnbull (Academic, New York, 1977), Vol. 32, pp. 1—86.

[20]P. Vashishta, P. Bhattacharyya, and K. S. Singwi, Phys. Rev. B **10**, 5108 (1974).

[21]This low-energy shift could be due to a lowering of the ground-state energy due to electron- (hole-) phonon interaction.

[22]E. Hanamura, J. Phys. Soc. Jpn. **39**, 1516 (1975); see also Ref. 1.

[23]D. L. Rode, in *Semiconductors and Semimetals,* edited by R. K. Willardson and A. C. Beer (Academic, New York, 1975), Vol. 10, pp. 1—89.

[24]The carrier velocity v can be approximately calculated according to $J=eD\,\mathrm{grad}N_{e\text{-}h}=e\bar{N}_{e\text{-}h}v$, where $\bar{N}_{e\text{-}h}$ is an average density. For $D=10$ cm^2/s, $N_{e\text{-}h}=7.7\times10^{18}$ cm^{-3}, $\Lambda/2=1.6$ μm, i.e., $\mathrm{grad}N_{e\text{-}h}=4.8\times10^{22}$ cm^{-4} and $\bar{N}_{e\text{-}h}=N_{e\text{-}h}/2$, we obtain $v=1.2\times10^5$ cm/s.

[25]An upper limit for the carrier velocity of $v=2.5\times10^6$ cm/s is reported in K. Kempf and C. Klingshirn, Solid State Commun. **49**, 23 (1984).